Electrical Double Layer

Effect of Electrolyte Concentration on the Stern Layer Thickness at a Charged Interface

Matthew A. Brown,* Alok Goel, and Zareen Abbas

Abstract: The chemistry and physics of charged interfaces is regulated by the structure of the electrical double layer (EDL). Herein we quantify the average thickness of the Stern layer at the silica (SiO_2) nanoparticle/aqueous electrolyte interface as a function of NaCl concentration following direct measurement of the nanoparticles' surface potential by X-ray photoelectron spectroscopy (XPS). We find the Stern layer compresses (becomes thinner) as the electrolyte concentration is increased. This finding provides a simple and intuitive picture of the EDL that explains the concurrent increase in surface charge density, but decrease in surface and zeta potentials, as the electrolyte concentration is increased.

When a solid surface comes into contact with an electrolyte solution, it often develops an excess charge. Ions in the adjacent electrolyte rearrange to screen this charge, forming an electrical double layer (EDL) in the process. The structure of the EDL, which is poorly understood at a microscopic level, is a topic of tremendous scientific debate because of its fundamental and technological significance across a breadth of active research fields.[1]

Several phenomenological models exist to describe the structure of the EDL, but the Gouy-Chapman–Stern (GCS) model finds widespread use within the chemical community because of its success in explaining many features of colloidal nanoparticles (NPs) in aqueous electrolyte solutions.[2] Within this model, the EDL of a colloid particle is characterized by a surface potential (Φ_{surf}), a Stern layer of finite thickness (d_{Stern}) bounded by the outer Helmholtz plane (OHP), surface (σ_{surf}) and outer Helmholtz plane charge densities (σ_{OHP}), a zeta potential (ζ), and a diffuse layer with Debye–Hückel screening length (λ_D; see Figure 1). σ_{surf} is measured by potentiometric titration[3] or FTIR spectroscopy,[4] whereas ζ is a calculated value based on electrophoretic mobility measurements[5] and assumes the potential at the start of the diffuse layer.[6] Φ_{surf} is the sum of the potential drop across the Stern layer (Φ_{Stern}^{drop}) and the potential of the diffuse layer (ζ),[7]

$$\Phi_{surf} = \Phi_{Stern}^{drop} + \zeta \tag{1}$$

Figure 1. Gouy-Chapman–Stern model of the electrical double layer showing the distribution of hydrated ions and water molecules, the Stern and diffuse layers, a negative surface charge density (SCD), and the potential profile as a function of distance from the charged surface (solid line). The zeta potential (ζ) is assumed as the potential at the start of the diffuse layer.[6]

and is accessible only by in situ X-ray photoelectron spectroscopy (XPS) for dispersed systems.[7,8] To our knowledge, d_{Stern} at an NP interface cannot be directly measured with any known analytical probe but is calculated under the assumption that there are no free ions in the Stern layer.[9] This impels the Stern layer to act as a parallel-plate capacitor with potential drop,

$$\Phi_{Stern}^{drop} = \sigma_{surf}(d_{Stern}/\varepsilon\varepsilon_0) \tag{2}$$

where ε is the dielectric constant of water at the interface, ε_0 the vacuum permittivity, and $\varepsilon\varepsilon_0/d_{Stern}$ the capacitance. Combining Equations (1) and (2) gives the average thickness of the Stern layer in terms of three measurable quantities: σ_{surf}, Φ_{surf}, and ζ.

$$d_{Stern} = (\varepsilon\varepsilon_0/\sigma_{surf})(\Phi_{surf}-\zeta) \tag{3}$$

With knowledge of d_{Stern}, a complete quantitative description of the EDL within the framework of the GCS model is realized.

Silica is amphoteric in aqueous solutions, and at pH values above the isoelectric point (ca. 2–4) it carries negative charge that results from deprotonation of surface bound hydroxy groups.[10] Our potentiometric titration results are consistent with a negative σ_{surf} at pH 10 that increases in magnitude with an increase in NaCl concentration (Figure 2a, Table 1). This trend is well-known from previous work on colloidal silica.[11] The nonporous[12] and surfactant (ligand) free structure of our 9 nm diameter[13] Ludox silica sample allows this negative

[*] Dr. M. A. Brown, A. Goel
    Laboratory for Surface Science and Technology, Department of Materials, ETH Zürich (Switzerland)
    E-mail: matthew.brown@mat.ethz.ch

    Prof. Dr. Z. Abbas
    Department of Chemistry and Molecular Biology, University of Gothenburg (Sweden)

    Supporting information for this article can be found under http://dx.doi.org/10.1002/anie.201512025.
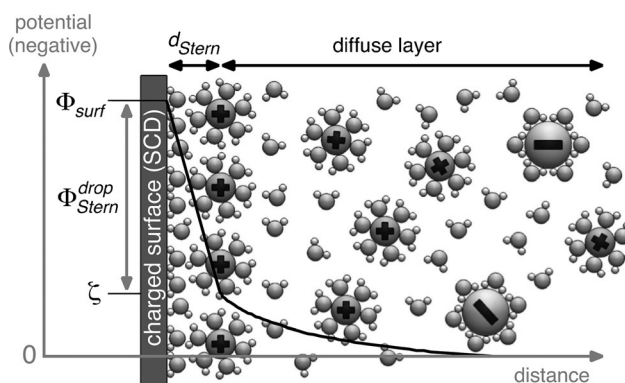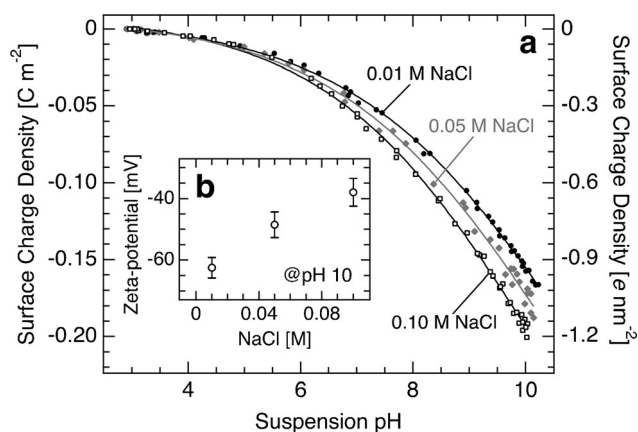
Figure 2. a) Surface charge density of 5 wt.% 9 nm Ludox colloidal silica in 0.01, 0.05, and 0.10 M NaCl as a function of bulk pH. Results (symbols) of three repeat experiments are shown. Solid lines are intended only as guides. b) Zeta potentials of 2 wt.% 9 nm Ludox colloidal silica in 0.01, 0.05, and 0.10 M NaCl at pH 10.

Table 1: Properties of the electrical double layer (EDL) at the silica NP-NaCl electrolyte interface at pH 10.[a]

NaCl [M]	σ_{surf} [C m^{-2}]	ζ-pot [mV]	σ_{DL} [C m^{-2}]	σ_{OHP} [C m^{-2}]	Φ_{surf} [mV]	d_{Stern} [Å]
0.01	−0.155	−62.5	0.027	0.128	−435	9.1
	(0.001)	(3.3)	(0.002)	(0.003)	(40)	(0.9)
0.05	−0.173	−48.5	0.036	0.137	−385	7.4
	(0.003)	(4.2)	(0.004)	(0.007)	(20)	(0.4)
0.10	−0.194	−37.9	0.036	0.158	−355	6.2
	(0.002)	(4.5)	(0.005)	(0.007)	(20)	(0.4)

[a] Numbers in brackets pertain to measurement errors.

charge to be uniquely assigned to the surface of the particles that are in direct contact with the aqueous electrolyte. With a typical silanol density of 4.6–4.9 OH nm^{-2} for amorphous silica,[14] our maximum determined surface charge density of −0.194 C m^{-2} (−1.21 e nm^{-2}) in 0.10 M NaCl corresponds to approximately 25% deprotonation.

Zeta potentials are calculated[5] from electrophoretic mobilities at pH 10 and reveal negative potential at the start of the diffuse layer (Figure 2 b, Table 1). The trend with increasing NaCl concentration is opposite to that of σ_{surf}, as ζ decreases in magnitude.[15] We subsequently used ζ to compute the charge density of the diffuse layer (σ_{DL}) by Gouy-Chapman theory. Using Ohshima's adaptation that accounts for the finite size of the NP,[6] we compute the electrokinetic charge density (σ_{EK}) with the relation $-\sigma_{EK} = \sigma_{DL}$, and find positive diffuse layer charge (Table 1).

Charge neutrality in the EDL ensures $\sigma_{surf} + \sigma_{OHP} + \sigma_{DL} = 0$, allowing the charge density of the OHP (σ_{OHP}) to be quickly determined. We find σ_{OHP} increases by $23 \pm 9\%$ going from 0.01 to 0.10 M NaCl, in quantitative agreement with the measured increase in σ_{surf} (Table 1). This result provides a microscopic description of the EDL that justifies the measured increase in σ_{surf} with NaCl concentration: increased co-adsorption of sodium at the OHP facilitates the deprotonation of surface silanol groups by providing enhanced screening of the charged sites.[16]
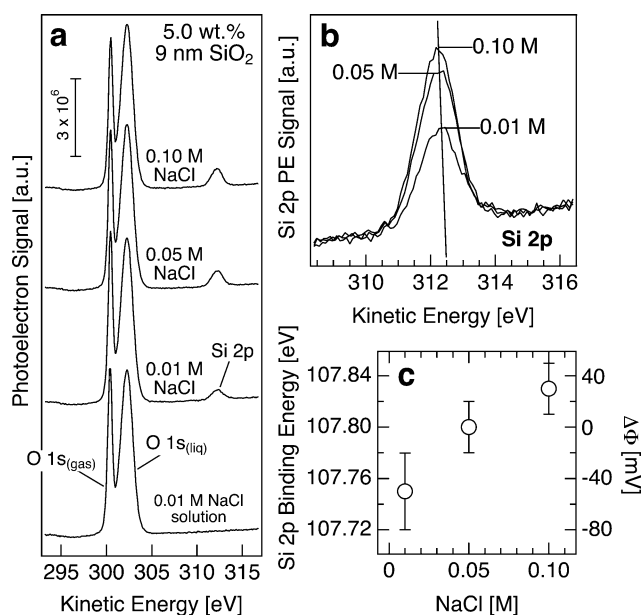

Figure 3. a) O 1s and Si 2p photoelectron spectra as a function of NaCl concentration. The bottom trace is a reference spectrum of 0.01 M NaCl (no silica NPs). b) Si 2p photoelectron spectra. c) Si 2p binding energy (left axis) and relative change in surface potential (right axis) as determined from curve fitting of the spectra of (b).

Using a liquid microjet[17] we measured O 1s and Si 2p XP spectra as a function of NaCl concentration (Figure 3 a). There are two peaks in the O 1s region; gas phase water at low KE (labeled O 1s$_{(gas)}$) and liquid water at higher KE (O 1s$_{(liq)}$).[18] The gas phase component originates from non-ideal overlap between the X-ray beam (fwhm = 100 µm)[18] and the liquid microjet (28 µm). Spectral overlap with liquid water prevents the oxygen component of the NPs from being detected.[12] Taking the binding energy (BE) of the O 1s$_{(liq)}$ peak as a reference, XPS reports directly on the change in NP surface potential ($\Delta\Phi_{surf}$) through the BE shift of the Si 2p orbital[7] with NaCl concentration (Figure 3 b).[19] Notably, this technique requires no a priori knowledge of the oxide surface or EDL structure since the shift in BE of the Si 2p level is directly proportional to $\Delta\Phi_{surf}$.[20] Quantifying the Si 2p BE relative to that in 0.05 M NaCl reveals that the surface potential shifts 50 mV lower (more negative) in 0.01 M and 30 mV higher (less negative) in 0.10 M NaCl (Figure 3 c). Absolute values of Φ_{surf} are determined using the relative shifts measured here and a reference surface potential of −385 mV in 0.05 M NaCl at pH 10, as recently determined by pH dependent XPS experiments.[7] Taken together we find that the surface potential of 9 nm colloidal silica at pH 10 is -435 ± 40 mV in 0.01 M, -385 ± 20 mV in 0.05 M, and -355 ± 20 mV in 0.10 M NaCl (Table 1).

Having determined σ_{surf}, ζ, and Φ_{surf}, the average thickness of the Stern layer is calculated from Equation (3) using ε for the water–silica interface (43.0).[21] We find d_{Stern} decreases with an increase in NaCl concentration; 9.1 ± 0.9 Å in 0.01 M, 7.4 ± 0.4 Å in 0.05 M, and 6.2 ± 0.4 Å in 0.10 M NaCl (Table 1). The capacitance of the Stern layer ($\varepsilon\varepsilon_0/d_{Stern}$) follows naturally; 0.42 F m^{-2} in 0.01 M, 0.51 F m^{-2} in 0.05 M, and 0.61 F m^{-2}

in 0.10 M NaCl. Numerical simulations of the EDL of spherical particles (ultramicroelectrodes) have shown that the Stern layer capacitance is independent of particle size,[22] suggesting our results are amenable to extended surfaces of amorphous silica.

The overwhelming effect of d_{Stern} on the electrostatics of the system is immediately evidenced by antipodal extremes of Φ_{surf} and σ_{surf}: Φ_{surf} is most negative when σ_{surf} is least negative, and vice versa (Table 1). This finding allows us to conclude that the magnitude of the surface potential at the silica/electrolyte interface is (essentially) set by the structure of the electrolyte solution, specifically the average thickness d_{Stern}, and not by the structure of the silica surface. This finding certainly extends to other oxide/electrolyte interfaces, as it makes intuitive, physical sense after recalling that the potential drop across a parallel-plate capacitor is a linear function of plate separation (in our case the two plates are represented by the NP surface and the OHP). In the GCS model of the EDL, two surfaces with identical charge density can have (very) different Φ_{surf} if d_{Stern} varies, making it clear that surface potentials cannot be accurately predicted using the Nernst equation.[2c, 23]

We are presently in a position to provide a microscopic description of the EDL that quantitatively justifies the measured decrease in ζ with increasing NaCl concentration. The origin of change in ζ stems uniquely from the larger capacitance of the Stern layer at higher electrolyte concentration, which leads to substantially lower surface potentials. Interestingly, for all NaCl concentrations investigated herein we find 85–90% of the overall potential drop occurs by the start of the diffuse layer.

The dependence of d_{Stern} on NaCl concentration suggests a relation with osmotic pressure (Π), which is calculated from the van't Hoff equation, $\Pi = MRT$, where M is the total local ion concentration at the OHP (mol L^{-1}), R the ideal gas constant, and T the temperature. The local co-ion (n_-) and counterion (n_+) concentrations in the diffuse layer fulfill Boltzmann distributions, $n_-(x) = n_0\exp(e\Phi(x)/k_{\text{B}}T)$ and $n_+(x) = n_0\exp(-e\Phi(x)/k_{\text{B}}T)$, where n_0 is the bulk NaCl concentration, e the elemental charge, and $\Phi(x)$ comes from the solution of the classical Poisson–Boltzmann equation (for $x \geq d_{\text{Stern}}$ and $\Phi(d_{\text{Stern}}) = \zeta$). The results for 0.05 M NaCl are shown in Figure 4a. We find total ion concentrations at the OHP of 0.11 M in 0.01 M, 0.33 M in 0.05 M, and 0.45 M in 0.10 M NaCl, with corresponding osmotic pressures of 258, 767, and 1051 kPa, respectively. A plot of d_{Stern} versus Π reveals a linear relationship (Figure 4b, coefficient of determination 0.996), and provides a simple and intuitive justification for the compression of the Stern layer at higher NaCl concentrations. That is, in going from 0.01 M to 0.10 M NaCl the osmotic pressure exerted on the OHP increases nearly four-fold, and the net result is a compression of d_{Stern}.

The average thickness of the Stern layer, determined herein, is proportional to the amplitude of the sum-frequency generation (SFG) OH stretch band assigned to under-coordinated water (ca. 3400 cm^{-1}, liquid-like) at the planar fused silica–NaCl electrolyte interface (Figure 5).[24] If we assume all water molecules within the Stern layer contribute equally to the SFG amplitude—a reasonable assumption
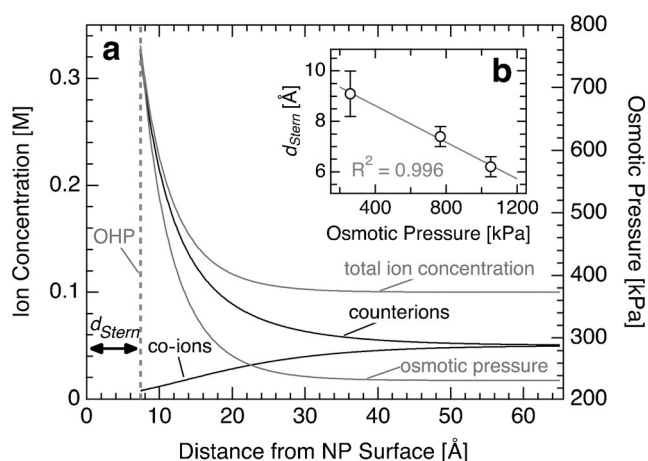

Figure 4. a) Co-, counter- and total ion concentrations at the silica/electrolyte interface in 0.05 M NaCl (left axis). Osmotic pressure determined from the total ion concentration (right axis). b) Stern layer thickness as a function of osmotic pressure at the outer Helmholtz plane (OHP). The solid line is a linear fit of the results.
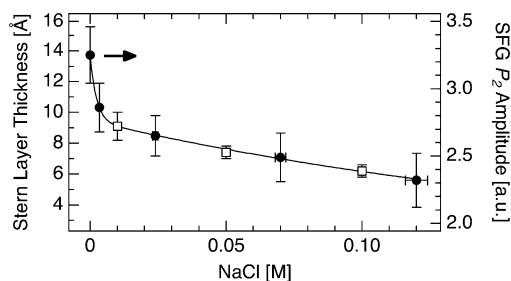

Figure 5. Left axis, open symbols: Stern layer thickness as derived from Equation (3). Right axis, closed symbols: Sum-frequency generation (SFG) peak amplitude of the OH stretch band assigned to under-coordinated water at the silica interface in NaCl electrolyte (*ssp* polarization, P_2 band at approximately 3400 cm^{-1}; see Table 1 in Ref. [24]).

considering Booth's model of water dielectric saturation[25] and recalling that the electric field inside a capacitor is constant—then the amplitude of the SFG signal can be thought of as a measure of the average thickness of the Stern layer, and quantitative agreement is, in fact, expected. However, our results provide a molecular level interpretation of the EDL yet to be proposed by the SFG community (Stern layer compression), but one that is fully supported by their independent measurements.

From a geometric structure standpoint, the implications of a varying d_{Stern} are easily understood after subtracting the radius of the sodium ion, Na^+_{hyd} (4.7 Å),[26] to reveal the average thickness of water hydrating the surface of NPs. We find thicknesses of 1.5 ± 0.4 Å in 0.10 M, 2.7 ± 0.4 Å in 0.05 M, and 4.4 ± 0.9 Å in 0.01 M NaCl, consistent with, on average, less than one, one, and more than one monolayer of water (ca. 3 Å[27]). In 0.10 M NaCl these findings imply that, on average, sodium ions at the OHP share part of their hydration shell with hydrating water molecules on the NPs surface and adsorption cannot be classified as purely non-specific. In

0.05 M NaCl, we find on average that d_{Stern} arises from one molecular layer of water that hydrates the NP surface and the hydrated sodium radius—a truly non-specific counterion adsorption. This one layer of water is broadly consistent with the molecular level interpretations of atomic force microscopy experiments that show a tightly bound hydration layer on negatively charged silica surfaces.[28] Non-specific adsorption also occurs in 0.01 M NaCl. Furthermore, if we assume that the trend of decreasing d_{Stern} with increasing NaCl concentration (osmotic pressure) extends beyond our measurement range, our results would lend support to the idea that Na$^+$ binds specifically at $\equiv$Si$-$O$^-$ sites in 0.35 M NaCl, as recently predicted by MD simulations.[29] However, because experiments are presently only capable of quantifying the average Stern layer thickness of the EDL, molecular simulations are needed that can account for complex potentials of mean force that include several local minima. These models could potentially describe the simultaneous presence of ions in different hydration environments at the surface that are averaged out in the experiments.

In summary, through a combination of X-ray photoelectron spectroscopy, potentiometric titration, and electrophoretic mobility experiments, the average thickness of the Stern layer at the silica NP-NaCl electrolyte interface was quantified. The concurrent increase in surface charge density and decrease in zeta potential that results from an increase in electrolyte concentration is explained within the Gouy-Chapman–Stern model by one simple observation: a compression of the Stern layer and a corresponding increase in its capacitance.

[1] a) M. F. Toney, J. N. Howard, J. Richer, G. L. Borges, J. G. Gordon, O. R. Melroy, D. G. Wiesler, D. Yee, L. B. Sorensen, *Nature* **1994**, *368*, 444–446; b) W. B. Russel, D. A. Saville, W. R. Schowalter, *Colloidal Dispersions*, Cambridge University Press, Cambridge, **1999**; c) W. Sparreboom, A. van den Berg, J. C. T. Eijkel, *Nat. Nanotechnol.* **2009**, *4*, 713–720; d) Y. Jiang, R. Tang, B. Duncan, Z. Jiang, B. Yan, R. Mout, V. M. Rotello, *Angew. Chem. Int. Ed.* **2015**, *54*, 506–510; *Angew. Chem.* **2015**, *127*, 516–520; e) B. E. Conway, *Electrochemical Supercapacitors: Scientific Fundamentals and Technological Applications*, Plenum Publishers, New York, **1999**; f) N. S. Choi, Z. H. Chen, S. A.

Freunberger, X. L. Ji, Y. K. Sun, K. Amine, G. Yushin, L. F. Nazar, J. Cho, P. G. Bruce, *Angew. Chem. Int. Ed.* **2012**, *51*, 9994–10024; *Angew. Chem.* **2012**, *124*, 10134–10166.

[2] a) T. Hiemstra, W. H. Van Riemsdijk, *J. Colloid Interface Sci.* **1996**, *179*, 488–508; b) J. Sonnefeld, *Colloid Polym. Sci.* **1995**, *273*, 932–938; c) I. Larson, P. Attard, *J. Colloid Interface Sci.* **2000**, *227*, 152–163.

[3] J. Lützenkirchen, T. Preočanin, D. Kovačević, V. Tomišić, L. Lövgren, N. Kallay, *Croat. Chem. Acta* **2012**, *84*, 391–417.

[4] T. Lagström, T. A. Gmür, L. Quaroni, A. Goel, M. A. Brown, *Langmuir* **2015**, *31*, 3621–3626.

[5] K. Makino, H. Ohshima, *Langmuir* **2010**, *26*, 18016–18019.

[6] a) D. J. Shaw, *Introduction to Colloid and Surface Chemistry*, Fourth ed., Butterworth-Heinemann Ltd., Oxford, **1992**; b) J. Lyklema, *J. Colloid Interface Sci.* **2015**, *446*, 335–343.

[7] M. A. Brown, Z. Abbas, A. Kleibert, A. Goel, S. May, T. M. Squires, *Phys. Rev.*, **2016**, *6*, 011007.

[8] M. A. Brown, A. Beloqui Redondo, M. Sterrer, B. Winter, G. Pacchioni, Z. Abbas, J. A. van Bokhoven, *Nano Lett.* **2013**, *13*, 5403–5407.

[9] "Solid-Liquid Interfaces": J. Lyklema, *Fundamentals of Interface and Colloid Science, Vol. II*, Academic Press, San Diego, **1995**.

[10] a) R. K. Iler, *The Chemistry of Silica: Solubility, Polymerization, Colloid and Surface Properties and Biochemistry of Silica*, Wiley, New York, **1979**; b) G. A. Parks, *Chem. Rev.* **1965**, *65*, 177–198.

[11] a) G. H. Bolt, *J. Phys. Chem.* **1957**, *61*, 1166–1169; b) S. K. Milonjić, *Colloid Surface* **1987**, *23*, 301–312; c) J. Sonnefeld, A. Gobel, W. Vogelsberger, *Colloid Polym. Sci.* **1995**, *273*, 926–931; d) T. F. Tadros, J. Lyklema, *J. Electroanal. Chem.* **1968**, *17*, 267–275.

[12] M. A. Brown, M. Arrigoni, F. Heroguel, A. Beloqui Redondo, L. Giordano, J. A. van Bokhoven, G. Pacchioni, *J. Phys. Chem. C* **2014**, *118*, 29007–29016.

[13] a) A. Beloqui Redondo, I. Jordan, I. Ziazadeh, A. Kleibert, J. B. Giorgi, H. J. Wörner, S. May, Z. Abbas, M. A. Brown, *J. Phys. Chem. C* **2015**, *119*, 2661–2668; b) M. A. Brown, N. Duyckaerts, A. Beloqui Redondo, I. Jordan, F. Nolting, A. Kleibert, M. Ammann, H. J. Wörner, J. A. van Bokhoven, Z. Abbas, *Langmuir* **2013**, *29*, 5023–5029.

[14] L. T. Zhuravlev, *Colloids Surf. A* **2000**, *173*, 1–38.

[15] G. V. Franks, *J. Colloid Interface Sci.* **2002**, *249*, 44–51.

[16] a) Z. Abbas, C. Labbez, S. Nordholm, E. Ahlberg, *J. Phys. Chem. C* **2008**, *112*, 5715–5723; b) L. Vayssieres, *J. Phys. Chem. C* **2009**, *113*, 4733–4736; c) M. Porus, C. Labbez, P. Maroni, M. Borkovec, *J. Chem. Phys.* **2011**, *135*, 064701.

[17] Any potential influence of streaming potentials associated with the operation of the liquid microjet can be ruled out because the Si 2p BEs are referenced to that of O 1s (assumed constant between the three solutions). Additionally, the continuously refreshed interface provided by the liquid microjet eliminates any possibility of X-ray beam damage having influence on the results.

[18] G. Olivieri, A. Goel, A. Kleibert, M. A. Brown, *J. Synchrotron Radiat.* **2015**, *22*, 1528–1530.

[19] The difference in Si 2p intensity between the three samples is easily accounted for by an effective radius that includes the physical size of the NP plus the Debye length.

[20] E. J. Crumlin, H. Bluhm, L. Zhi, *J. Electron Spectrosc. Relat. Phenom.* **2013**, *190*, 84–92.

[21] D. A. Sverjensky, *Geochim. Cosmochim. Acta* **2005**, *69*, 225–257.

[22] H. N. Wang, L. Pilon, *J. Phys. Chem. C* **2011**, *115*, 16711–16719.

[23] B. J. Kirby, *Micro- and Nanoscale Fluid Mechanics. Transport in Microfluidic Devices*, Cambridge University Press, New York, NY, **2013**.

[24] K. C. Jena, D. K. Hore, *J. Phys. Chem. C* **2009**, *113*, 15364–15372.

[25] F. Booth, *J. Chem. Phys.* **1951**, *19*, 391–394.

[26] J. Kielland, *J. Am. Chem. Soc.* **1937**, *59*, 1675–1678.

[27] a) D. Argyris, A. Phan, A. Striolo, P. D. Ashby, *J. Phys. Chem. C* **2013**, *117*, 10433–10444; b) A. Poynor, L. Hong, I. K. Robinson, S. Granick, Z. Zhang, P. A. Fenter, *Phys. Rev. Lett.* **2006**, *97*, 266101.

[28] J. Morag, M. Dishon, U. Sivan, *Langmuir* **2013**, *29*, 6317–6322.

[29] S. Dewan, V. Carnevale, A. Bankura, A. Eftekhari-Bafrooei, G. Fiorin, M. L. Klein, E. Borguet, *Langmuir* **2014**, *30*, 8056–8065.